MOTION ARTEFACT REMOVAL IN FUNCTIONAL NEAR-INFRARED SPECTROSCOPY SIGNALS BASED ON ROBUST ESTIMATION

Mengmeng Wang, Abd-Krim Seghouane

Department of Electrical and Electronic Engineering
The University of Melbourne, Australia

ABSTRACT

Functional Near-InfraRed Spectroscopy (fNIRS) has gained widespread acceptance as a non-invasive neuroimaging modality for monitoring functional brain activities. fNIRS uses light in the near infra-red spectrum (600-900 nm) to penetrate human brain tissues and estimates the oxygenation conditions based on the proportion of light absorbed. In order to get reliable results, artefacts and noise need to be separated from fNIRS physiological signals. This paper focuses on removing motion-related artefacts. A new motion artefact removal algorithm based on robust parameter estimation is proposed. Results illustrate that the proposed algorithm can outperform the state-of-art algorithms in removing motion artefacts. Moreover, the proposed algorithm is robust in estimating the parameters under different interference conditions.

Index Terms— fNIRS, motion artefact removal, robust estimation

1. INTRODUCTION

Functional Near Infrared Spectroscopy (fNIRS) is a non-invasive neuroimaging modality for monitoring functional brain activities [8, 23]. fNIRS exploits the property of 'optical window' in which biological tissues are relatively transparent. fNIRS uses light in the near infra-red spectrum (600-900nm) to penetrate human brain tissue using optical sources and detectors and estimates the brain oxygenation conditions [10]. fNIRS measures the changes of optical densities and calculates the concentration changes of oxyhaemoglobin (HbO) and deoxyhaemoglobin (HbR) using modified Beer-Lambert law (MBLL) [13]. fNIRS has the advantages of portable, low-cost, and little restriction on movements compared to other functional neuroimaging modalities. It is widely used in cognitive studies, language development, infant monitoring and other functional analyses [21].

fNIRS signals are subtle brain signals that reflect brain oxygenation conditions. Any interference or noise will cause variations of the fNIRS signals. In fNIRS functional analyses, signal preprocessing is essential in order to remove artefacts and noise from the signals. Motion artefacts are considered as one of the main types of signal artefacts in fNIRS signals [3]. Motion-related artefacts arise from the movements of the subjects' heads or eyebrows, which will cause the changes in blood circulation and the displacements between sources or detectors and the scalp. In fNIRS, motion artefacts will lead to sudden changes in the measured light intensities, and they will affect the results of functional analyses [11].

A significant amount of research in fNIRS signal processing in the past twenty years has been dedicated to motion artefact removal. Existing motion artefact removal methods include artefact rejection or adaptive filtering, which typically require additional hardware and probes. Alternatively, some methods use existing data without requiring additional hardware; such as Wiener filtering [4], Kalman filtering [5], Principle Component Analysis (PCA) [22][14], Spline Interpolation (SI) [12] and Discrete Wavelet Transformation (DWT) [9]. Some methods take use of the HbO and HbR correlation hypothesis, including Correlation-Based Signal Improvement (CBSI) [2] and Independent Component Analysis (ICA) [20]. More recently, the Transient Artifact Reduction Algorithm (TARA) [16, 17] has been proposed to model signal and motion artefacts by setting sparsity constraints on motion artefacts.

In this paper, with the utilisation of artefact characteristics, we propose a motion artefact removal algorithm based on robust estimation with reduced basis functions and weighted parameter estimation method. We test the performance of the proposed algorithm using experimental data. Results show that the proposed algorithm can successfully remove or reduce motion-related artefacts in the signals. More importantly, the algorithm is robust under different interference conditions.

The rest of the paper is organised as follows. Section 2 presents the proposed motion artefact removal algorithm. In Section 3, the results of the proposed algorithm are presented and discussed. Finally, in Section 4, the conclusions are presented.

2. PROPOSED ALGORITHM

2.1. fNIRS Model

The signal $\mathbf{y}$ represents a single-channel fNIRS signal measuring the changes of concentrations in HbO or HbR. The

vector $\mathbf{y}$ contains fNIRS haemodynamic response signal of length N, where N represents the number of time stamps. The signal can be modelled as in

$$\mathbf{y} = \mathbf{x} + \mathbf{e}, \quad \mathbf{y}, \mathbf{x}, \mathbf{e} \in \mathbb{R}^N \tag{1}$$

where $\mathbf{y}$, $\mathbf{x}$, $\mathbf{e}$ represent the fNIRS detected signal (contains artefacts), true physiological response, and artefact term.
The artefact term $\mathbf{e}$ contains motion artefacts and noise in fNIRS signals. We consider the physiological effects caused by the heart or respiration to be the global effects and they are part of signal $\mathbf{x}$. We model the motion artefacts as the summation of spike-shaped and square-shaped artefacts [16]. Spikes represent short-term motion artefacts, while square functions represent long-term artefacts. Our aim is to remove the artefact term $\mathbf{e}$ by estimating the physiological signal $\mathbf{x}$.

2.2. Problem Formulation

The physiological signal $\mathbf{x}$ can be represented by the linear model

$$\mathbf{y} = \mathbf{B}\,\boldsymbol{\theta} + \mathbf{e} \tag{2}$$

where $\mathbf{B}$ is a basis matrix ($N \times m$) consisting m basis functions. $\boldsymbol{\theta}$, of dimension ($m \times 1$), represents unknown parameters that we want to estimate [1]. The inverse DCT matrix, which is equivalent to the transpose of the forward DCT, denotes as the matrix $\mathbf{B}$ in (2). In the proposed algorithm, DCT bases is used to represent different frequency components in the signals [6].
To estimate the signal, we select the r highest DCT coefficients, where are denoted as $\boldsymbol{\theta}_r \in \mathbb{R}^r$. Then the columns corresponding to $\boldsymbol{\theta}_r$ are selected from $\mathbf{B}_{idct}$ to form the reduced basis matrix $\mathbf{B}_r$. $\mathbf{B}_r$ has the dimension of $(N \times r)$. Therefore, (2) can be rewritten into

$$\mathbf{y} = \mathbf{B}_r\,\boldsymbol{\theta}_r + \mathbf{e} \tag{3}$$

In order to remove long-term artefacts, we use the Difference-Based Estimation (DBE) technique proposed in [18][19][15], which uses the first-order difference of $\mathbf{y}$ to estimate $\boldsymbol{\theta}_r$

$$\tilde{\mathbf{y}} = \tilde{\mathbf{B}}_r\,\boldsymbol{\theta}_r + \tilde{\mathbf{e}} \tag{4}$$

where $\tilde{\mathbf{y}}$, $\tilde{\mathbf{B}}_r$ and $\tilde{\mathbf{e}}$ represent the first-order differences for the signal, basis matrix and noise respectively [18].

2.3. Parameter Estimation

Recall that the solution for (4) using Least-Squares (LS) estimation can be represented as in

$$\hat{\boldsymbol{\theta}}_{\mathrm{r-LS}} = (\tilde{\mathbf{B}}_r^\top \tilde{\mathbf{B}}_r)^{-1} \tilde{\mathbf{B}}_r^\top \tilde{\mathbf{y}} \tag{5}$$

Based on our assumption of the motion artefacts, $\tilde{\mathbf{e}}$ can be represented as positive and negative spikes, which yields outliers in the histogram or probability density function of the first-order signal difference $\tilde{\mathbf{y}}$. The LS solution in (5) is no longer appropriate in estimating the parameters because of its sensitivity to outliers.
In this paper, we obtain a robust estimate $\hat{\boldsymbol{\theta}}_\alpha$ by solving

$$\hat{\boldsymbol{\theta}}_\alpha = \underset{\mathbf{h}}{\operatorname{argmin}}\, L_\alpha(\boldsymbol{\theta}) = \underset{\boldsymbol{\theta}}{\operatorname{argmin}}\, \frac{1}{N-1} \sum_{i=1}^{N-1} \rho_\alpha \left\{ \frac{\tilde{y}_i - \mathbf{b}_i^\top \boldsymbol{\theta}}{\sigma} \right\} \tag{6}$$

where ρ_α is the robust loss function

$$\rho_\alpha(v) = \alpha^{-1} \left\{ 1 - \exp\left(-\alpha v^2/2\right) \right\},\ \alpha > 0. \tag{7}$$

For $\alpha = 0$ the limit $\alpha \to 0$, this $\rho_\alpha(v) \to \rho_0(v) = v^2/2$ for any $v \geq 0$, which corresponds to the familiar quadratic loss $L_\alpha(\boldsymbol{\theta}) = \sum_{i=1}^{N-1} \{(\tilde{y}_i - \mathbf{b}_i^\top \boldsymbol{\theta})^2 / 2\sigma^2\}$. The quadratic loss is described above for estimating θ but offer no protection against anomalous observations which could be frequent in fNIRS. The general case with $\alpha \neq 0$ corresponds to a weighted estimation that tends to down weight the errors that are far from the nominal density, thus removing outliers.
More insight can be gained by differentiating the objective (8). This gives the weighted least squares estimating equations

$$0 = \sum_{i=1}^{N-1} w_i(\boldsymbol{\theta}, \mathbf{B}; \alpha) \frac{\mathrm{d}}{\mathrm{d}\boldsymbol{\theta}} \left(\frac{\tilde{y}_i - \mathbf{b}_i^\top \boldsymbol{\theta}}{\sqrt{2}\sigma} \right)^2 \tag{8}$$

where the weights are given by

$$w_i(\boldsymbol{\theta}, \mathbf{B}; \alpha) = \exp\left\{ -\frac{\alpha}{2} \left(\frac{\tilde{y}_i - \mathbf{b}_i^\top \boldsymbol{\theta}}{\sigma} \right)^2 \right\} \tag{9}$$

In the special case $\alpha = 0$, we have uniform weights $w_1 = \cdots = w_{N-1} = 1$ and the corresponding estimator $\hat{\mathbf{h}}_{\mathbf{0}}$ is just the least squares estimator. On the other hand if $\alpha > 0$, an observation $\tilde{y}_i$ far from the mean $\mathbf{b}_i^\top \boldsymbol{\theta}$ receives relatively low weight compared to observations near the mean. Due to the form of the weights, anomalous observations far from the bulk of the data are automatically downweighted and have little impact on the final estimate which makes the estimator robust to outliers.
From now on it will be assumed that $\hat{\sigma}^2$ is known or has been estimated previously using

$$\hat{\sigma}^2 = \frac{1}{N-2} \sum_{i=1}^{N-1} \tilde{w}_i(\hat{\boldsymbol{\theta}}, \mathbf{B}; \alpha) \left(\tilde{y}_i - \mathbf{b}_i^\top \boldsymbol{\theta} \right)^2$$

where $\tilde{w}_i(\hat{\boldsymbol{\theta}}, \mathbf{B}; \alpha) = w_i(\boldsymbol{\theta}, \mathbf{B}; \alpha) / \sum_{i=1}^{N-1} w_i(\boldsymbol{\theta}, \mathbf{B}; \alpha)$ is defined in (9) or any other robust variance estimator [7]. In this paper it is taken equal to one as this generates good results.

$$\hat{\boldsymbol{\theta}}_\alpha = (\tilde{\mathbf{B}}_r^\top \mathbf{W} \tilde{\mathbf{B}}_r)^{-1} \tilde{\mathbf{B}}_r^\top \mathbf{W} \tilde{\mathbf{y}} \tag{10}$$

where the weighted matrix $\mathbf{W}$ is the diagonal matrix with w_i being the diagonal entries.

Note that the entries w_i in $\mathbf{W}$ also depend on the values of the parameter $\boldsymbol{\theta}$. Therefore, there is no close form solution for $\hat{\boldsymbol{\theta}}_\alpha$. Instead, the $\hat{\boldsymbol{\theta}}_\alpha$ can be calculated iteratively, where initial value is obtained using LS.

The true fNIRS signal after motion artefact removal can be estimated as

$$\hat{\mathbf{x}}_{\boldsymbol{\theta}_\alpha} = \mathbf{B}_r \hat{\boldsymbol{\theta}}_\alpha \tag{11}$$

2.4. Algorithm Integration

The proposed motion artefact removal algorithm is described in Algorithm 1. Two parameters need to be defined in the proposed algorithm, the number of basis functions selected from the basis matrix (r) and the robust estimation turning parameter (α). The value of r is related to how well the measured signal can be modelled using the basis functions. In practice, we choose a certain percentage of the DCT coefficients and their corresponding basis functions. The value of α is the tuning parameter which controls the amount of artefacts or outliers the algorithm can remove. α is tuned based on grid-search.

Algorithm 1 Proposed Motion Artefact Removal Algorithm

Input: $\mathbf{y}$, $\mathbf{B}_{dct}$, r, α
1: $\boldsymbol{\theta}_{dct} = \mathbf{B}_{dct}\ \mathbf{y}$
2: **for** n = 1 to r **do**
3: Find $d_n = \text{index}(max(\boldsymbol{\theta}_{dct}))$
4: $\mathbf{B}_{r.n} = \mathbf{B}_{dct.d}^\top$
5: **end for**
6: **for** i = 1 to N-1 **do**
7: $\tilde{y}_i = y(i+1) - y(i)$
8: $\tilde{\mathbf{B}}_{r_i.} = \mathbf{B}_{r_{(i+1).}} - \mathbf{B}_{r_i.}$
9: **end for**
10: LS Solution $\hat{\boldsymbol{\theta}}_{\text{LS}} = (\tilde{\mathbf{B}}_r^\top \tilde{\mathbf{B}}_r)^{-1} \tilde{\mathbf{B}}_r^\top \tilde{\mathbf{y}}$
11: Define the i-th row of $\tilde{\mathbf{B}}_r$: $\tilde{\mathbf{B}}_{r_i.} = \tilde{\mathbf{b}}_i$;
12: Starting with: $\boldsymbol{\theta}_\alpha = \hat{\boldsymbol{\theta}}_{\text{LS}}$
13: **for** t = 1 to T Iterations **do**
14: $w_{i,t} = \exp(-\alpha(\tilde{y}_i - \tilde{\mathbf{b}}_i \boldsymbol{\theta}_\alpha)^2)$
15: $\mathbf{W}_t = diag(w_{i,t})$
16: Update $\hat{\boldsymbol{\theta}}_\alpha = (\tilde{\mathbf{B}}_r^\top \mathbf{W}_t \tilde{\mathbf{B}}_r)^{-1} \tilde{\mathbf{B}}_r^\top \mathbf{W}_t \tilde{\mathbf{y}}$
17: **end for**
18: $\hat{\mathbf{x}}_{\boldsymbol{\theta}_\alpha} = \mathbf{B}_r \hat{\boldsymbol{\theta}}_\alpha$
Output: $\hat{\boldsymbol{\theta}}_\alpha$, $\hat{\mathbf{x}}_{\boldsymbol{\theta}_\alpha}$

3. RESULTS AND DISCUSSION

Resting-state fNIRS data was collected from young subjects (ages ranging from 3 to 12 years old). Data was collected using a NIRScout (NIRx) device at sampling frequency of 12.5Hz. One channel of HbO signal ($N = 4,500$) is used as the true resting-state data. The proposed algorithm can be applied channel-by-channel for multi-channel HbO signals.

Simulated motion artefacts are added to the resting state fNIRS data. In this example, we add six spike-shaped waves and three square-shaped waves with randomly generated amplitudes to the experimental signal in order to represent motion artefacts. The chosen numbers of the additive motion artefacts are used to simulate real movement conditions [16].

A windowing function is used to divide the experimental data into smaller windows. Windowing is used to limit the number of bases in $\mathbf{B}$ as well as to reduce the computational complexity. In this example, we choose window size $W = 200$, within each contains approximately 20s signal. The reduced basis coefficient is set to $r = 0.1 \times W$ and the α coefficient is set to $\alpha = 10$. The parameters r and α are set based on grid-search to obtain optimum results.

We compare the proposed algorithm with the state-of-art algorithm TARA [16]. The authors introduced two TARA algorithms which are used for convex and non-convex problems. We compare the proposed algorithm with both of the two TARA algorithms, denoted as TARA and TARA (Non-convex) in the figures. The example in Figure 1 shows a comparison between the proposed algorithm and TARA in removing motion artefacts. The description and implementation of TARA can be found in [16] and the author's homepage.

From Figure 1, both TARA and the proposed algorithm can successfully remove most of the added artefacts. In this particular example, TARA and TARA (Non-Convex) can give more precise results for the first $n =$ 2,500 data points. However, after $n =$ 2,500, TARA and TARA (Non-Convex) tend to give inaccurate results due to the added motion artefacts. That is mainly because TARA and TARA (Non-Convex) use an indirect approach by estimating the motion artefacts and then subtracting them from the measured signal. Our proposed algorithm, on the other hand, estimates the parameters directly and reconstructs the signals. For the proposed algorithm, as shown in Figure 1, the frequency oscillations of the estimated signal are preserved without losing any physiological information. The signal being removed is mainly high frequency noise which will not have impact on the physiological analysis of the signal.

To evaluate robustness, we run the proposed algorithm and TARA 100 times with randomly generated motion artefacts and calculate the mean value and standard deviation of the mean squared errors (MSEs). MSE measures the differences between the true resting-state signals and reconstructed signals. $\text{MSE} = \frac{1}{N}\sum_{i=1}^{N}(x_i - \hat{x}_i)^2$.

Signal-to-Interference Ratio (SIR) is defined as the ratio of the power of signal differences to the power of artefact differences (interference) $\text{SIR} = 10\log(P_{\tilde{\mathbf{x}}}/P_{\tilde{\mathbf{e}}})$. The SIR between the signal and motion artefacts is kept the same at SIR = 16 dB for all iterations. Within each iteration, motion artefacts with different amplitudes are spread randomly over the experimental data. MSEs are calculated by comparing the resting-state experimental data before adding motion artefacts with the estimated signal after applying motion artefact removal

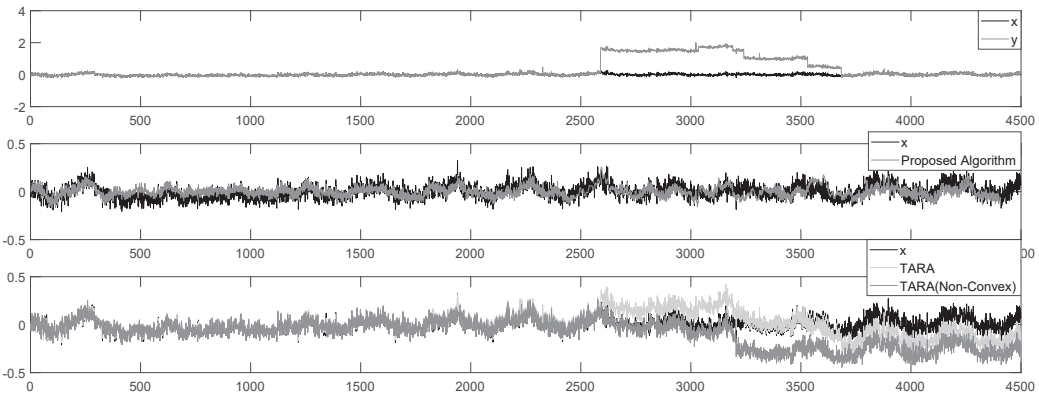

Fig. 1: Example results. Top: Experimental data ($\mathbf{x}$) and experimental data with motion artefacts ($\mathbf{y}$). Middle: Experimental data ($\mathbf{x}$) and the estimated signal from the proposed algorithm ($\hat{\mathbf{x}}_{\boldsymbol{\theta}_\alpha}$). Bottom: Experimental data ($\mathbf{x}$) and the estimated signal from the TARA and TARA (Non-Convex).

Table 1: The performance of the proposed algorithm under different conditions of SIR (MSEs).

		SIR=20 dB	SIR=18 dB	SIR=16 dB	SIR=14 dB	SIR=10 dB
TARA	Mean	0.0041	0.0114	0.0209	0.0499	0.1539
	Deviation	0.0040	0.0127	0.0150	0.0420	0.0917
TARA (Non-Convex)	Mean	0.0048	0.0119	0.0155	0.0440	0.1198
	Deviation	0.0060	0.0192	0.0159	0.0421	0.0999
Proposed	Mean	**0.0031**	**0.0034**	**0.0037**	**0.0043**	**0.0058**
	Deviation	**0.0001**	**0.0002**	**0.0002**	**0.0004**	**0.0006**

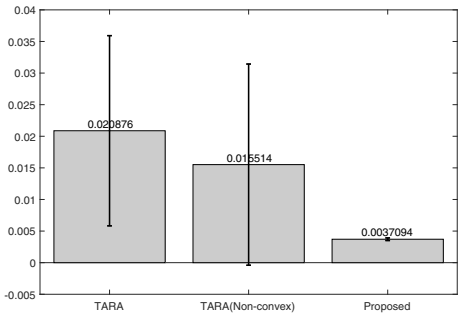

Fig. 2: Mean and standard deviation of MSEs for TARA, TARA (Non-Convex) and the proposed algorithm using experimental data. The bar chart represent the mean values of MSEs, the error bars along each bars represent the standard deviation of MSEs.

algorithms.

The results of the mean and standard deviation values of MSEs for the proposed algorithm and TARA are shown in Figure 2. TARA, TARA (Non-Convex) and the proposed algorithm have the mean values of MSEs of 0.0209, 0.0155 and 0.0037, respectively. The proposed algorithm achieves the best performance among all three algorithms in removing motion artefacts. Moreover, the robustness of the proposed algorithm is more prominent from Figure 2, the standard derivation of the proposed algorithm is insignificant. Results show that the proposed algorithm is more robust and stable compared to other algorithms, the shapes of the artefacts do not affect the performance of the proposed algorithm. Although for some cases TARA (Non-Convex) has better results in removing the motion artefacts, however, the algorithm is not robust and cannot be applied to general cases because of the high standard deviation.

We also compare the performance of the proposed algorithm for different interference conditions (SIRs). The results for performance comparison are shown in Table 1. Different SIR conditions denote different levels of motion artefacts. It is shown in Table 1 that under different SIRs, the proposed algorithm can achieve the best results with the lowest mean MSEs and standard derivations among all three algorithms.

4. CONCLUSION

In order to remove motion-related artefacts in fNIRS signals, a robust motion artefact removal algorithm is proposed in this paper. The proposed algorithm combines reduced basis functions with robust parameter estimation. We evaluate the performance using experimental fNIRS data with the added motion artefacts. Results show that the proposed algorithm can achieve good results in motion artefact removal performance and as well as robustness. Future work will focus on applying the proposed algorithm to signals with real motion artefacts and refining the parameter tuning in the proposed algorithm.

References

[1] C. M. Bishop, *Pattern Recognition and Machine Learning (Information Science and Statistics)*. Berlin, Heidelberg: Springer-Verlag, 2006, ISBN: 978-0-387-31073-2.

[2] X. Cui, S. Bray, and A. L. Reiss, "Functional near infrared spectroscopy (NIRS) signal improvement based on negative correlation between oxygenated and deoxygenated hemoglobin dynamics," *NeuroImage*, vol. 49, no. 4, pp. 3039–3046, Feb. 2010.

[3] T. J. Huppert, S. G. Diamond, M. A. Franceschini, and D. A. Boas, "HomER: a review of time-series analysis methods for near-infrared spectroscopy of the brain," *Applied optics*, vol. 48, no. 10, pp. D280–D298, Apr. 2009.

[4] M. Izzetoglu, A. Devaraj, S. Bunce, and B. Onaral, "Motion artifact cancellation in NIR spectroscopy using Wiener filtering," *IEEE Transactions on Biomedical Engineering*, vol. 52, no. 5, pp. 934–938, May 2005.

[5] M. Izzetoglu, P. Chitrapu, S. Bunce, and B. Onaral, "Motion artifact cancellation in NIR spectroscopy using discrete Kalman filtering," *Biomedical Engineering Online*, vol. 9, pp. 16-1–16-8, Mar. 2010.

[6] S. A. Khayam, "The discrete cosine transform (dct): theory and application," *Michigan State University*, vol. 114, pp. 1–31, 2003.

[7] R. A. Maronna, D. R. Martin, and V. J. Yohai, *Robust Statistics: Theory and Methods*. New York: John Wiley and Sons, 2006, ISBN: 978-0-470-01092-1.

[8] M. C. McKay, A. Shah, A. K. Seghouane, X. Zhou, W. Cross, and R. Litovsky, "Connectivity in language areas of the brain in cochlear implant users as revealed by fNIRS," *Advances in Experimental Medicine and Technology*, vol. 67, pp. 327–335, 2016.

[9] B. Molavi and G. A. Dumont, "Wavelet-based motion artifact removal for functional near-infrared spectroscopy," *Physiological Measurement*, vol. 33, no. 2, pp. 259–270, Feb. 2012.

[10] S. M. Musa, *Computational Optical Biomedical Spectroscopy and Imaging*. CRC Press, Jan. 2015, ISBN: 978-1-4822-3082-6.

[11] F. C. Robertson, T. S. Douglas, and E. M. Meintjes, "Motion Artifact Removal for Functional Near Infrared Spectroscopy: A Comparison of Methods," *IEEE Transactions on Biomedical Engineering*, vol. 57, no. 6, pp. 1377–1387, Jun. 2010.

[12] F. Scholkmann, S. Spichtig, T. Muehlemann, and M. Wolf, "How to detect and reduce movement artifacts in near-infrared imaging using moving standard deviation and spline interpolation," *Physiological Measurement*, vol. 31, no. 5, pp. 649–662, May 2010.

[13] F. Scholkmann, S. Kleiser, A. J. Metz, R. Zimmermann, J. Mata Pavia, U. Wolf, and M. Wolf, "A review on continuous wave functional near-infrared spectroscopy and imaging instrumentation and methodology," *NeuroImage*, vol. 85, Part 1, pp. 6–27, Jan. 2014.

[14] A. K. Seghouane and A. Cichocki, "Bayesian estimation of the number of principal components," *Signal Processing*, vol. 87, pp. 562–568, 2007.

[15] A. K. Seghouane and D. Ferrari, "Robust hemodynamic response function estimation from fnirs signals," *IEEE Transactions on Signal Processing*, vol. 67, pp. 1–11, 2019.

[16] I. W. Selesnick, H. L. Graber, Y. Ding, T. Zhang, and R. L. Barbour, "Transient Artifact Reduction Algorithm (TARA) Based on Sparse Optimization," *IEEE Transactions on Signal Processing*, vol. 62, no. 24, pp. 6596–6611, Dec. 2014.

[17] I. W. Selesnick, H. L. Graber, D. S. Pfeil, and R. L. Barbour, "Simultaneous Low-Pass Filtering and Total Variation Denoising," *IEEE Transactions on Signal Processing*, vol. 62, no. 5, pp. 1109–1124, Mar. 2014.

[18] A. Shah and A. Seghouane, "Consistent estimation of the hemodynamic response function in fNIRS," in *2013 IEEE International Conference on Acoustics, Speech and Signal Processing*, May 2013, pp. 1281–1285.

[19] A. Shah and A. K. Seghouane, "An integrated framework for joint HRF and drift estimation and HbO/HbR signal improvement in fNIRS data," *IEEE Transactions on Medical Imaging*, vol. 33, pp. 2086–2097, 2014.

[20] Y. Shi, G. Sun, H. Wang, Y. Leng, Y. Yang, and S. Ge, "Motion artifacts removal for fNIRS data based on independent component analysis," in *2015 12th International Computer Conference on Wavelet Active Media Technology and Information Processing (ICCWAMTIP)*, Dec. 2015, pp. 40–43.

[21] M. Strait and M. Scheutz, "What we can and cannot (yet) do with functional near infrared spectroscopy," *Frontiers in Neuroscience*, vol. 8, pp. 117-1–117-12, May 2014.

[22] Y. Zhang, D. H. Brooks, M. A. Franceschini, and D. A. Boas, "Eigenvector-based spatial filtering for reduction of physiological interference in diffuse optical imaging," *Journal of Biomedical Optics*, vol. 10, no. 1, pp. 11 014-1–11 014-11, Feb. 2005.

[23] X. Zhou, A. K. Seghouane, A. Shah, H. Innes-Brown, W. Cross, R. Litovski, and C. M. McKay, "Cortical speech processing in postlingually deaf adult cochlear implant users, as revealed by functional near-infrared spectroscopy," *Trends in Hearing*, vol. 22, pp. 1–18, 2018.